A Hybrid Correlation-Dicke Radiometer for Internal Body Thermometry

Jooeun Lee, Gabriel Santamaria Botello, Robert Streeter, Kaitlin Hall, Zoya Popović
University of Colorado Boulder, USA
{jooeun.lee, gabriel.santamariaBotello, robert.streeter, kaitlin.hall, zoya}@colorado.edu

***Abstract* — In this paper, we present a compact calibrated radiometer for measuring internal body temperature. The radiometer architecture combines the benefits of a correlation and a Dicke radiometer. The sensitivity to load impedance variations is reduced through a balanced topology, while the pre-detection switch reduces sensitivity to gain fluctuations of all components in the receive chain that follows. The radiometer is designed to operate in the 1.4–1.427 GHz quiet band using off-the-shelf components on a 10 cm×7.6 cm printed circuit board. Two types of temperature estimation methods are compared and the errors analyzed using resistors at known controllable temperatures at both input ports. One of the ports is then connected to a near-field antenna probe matched to tissue layers of the cheek. When water of variable temperature is in the mouth, an independent thermocouple verifies the radiometric temperature of the water measured by the probe placed on the skin.**

***Keywords* — Radiometer, thermometry, sensitivity, calibration.**

I. Introduction

There are a number of medical applications that can benefit from knowledge of internal tissue temperature, ranging from surgical and therapeutic to wellness. For example, during cardiac surgery the brain is cooled to 15°C when the blood supply is cut off, and needs to be brought to normal temperature within 30 minutes [1]. On the other hand, during hyperthermia for cancer treatment, the temperature of tissues is increased [2]. Sleep disorders are also related to internal body temperature. 60 million U.S. adults report frequent difficulty sleeping, resulting in an estimated annual indirect costs from insomnia due to loss of productivity of $60 billion. The core body temperature (CBT) is synchronized with melatonin and sleep propensity, e.g. [3], and monitoring CBT can help with sleep disorder treatment. A number of other applications, such as monitoring infections, joint inflammation, muscle temperature during heavy exercise, etc., can benefit from the knowledge of internal tissue temperature.

Current methods to measure internal temperature include nasal and rectal measurements, invasive methods (e.g. needle probes), non-reusable pills that measure intestine temperature, expensive and large MRI, as well as heat-flux devices for sub-cm depth [4] [5]. Alternatively, microwave radiometry can be used to measure the total thermal noise power emitted from a stack of tissues, and the temperature of a specific layer can be estimated, e.g. [6]–[9].

Different well-known radiometer types [10] have been studied for measuring internal temperature, including the Dicke radiometer [11] and correlation radiometer [12]. The Dicke radiometer has a switch after the antenna which allows calibration for gain fluctuations by measuring one or more known reference temperature loads. However, the insertion loss of the switch increases the noise figure, and the time on-target is reduced based on the switching duty cycle. The correlation radiometer uses a balanced hybrid coupler architecture with two low-noise gain paths, and has the advantages of continuous measurement of both the target and reference, and lower sensitivity to impedance mismatches at the inputs.

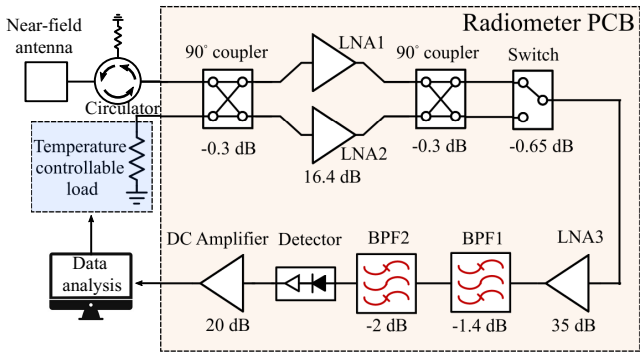

Fig. 1. Block diagram of the correlation-Dicke hybrid radiometer for internal tissue thermometry. The input to the correlation portion of the radiometer is total thermal noise received by a near-field antenna placed on the skin. The radiometer is calibrated using a temperature-controllable 50-Ω load. The switch toggles between the two paths to calibrate gain fluctuation of the pre-detection stage.

Here we introduce a radiometer architecture shown in Fig. 1, which is a hybrid between a correlation and Dicke radiometer, with the benefits of less sensitivity to load impedance variations, while the pre-detection switch reduces sensitivity to gain fluctuations of components after the switch. The radiometer is implemented with commercially-available off-the-shelf components for operation in the 1.4-1.427 GHz band. After characterization with a known-temperature matched load and a variable-temperature matched reference, the radiometer is used to track temperature in a human mouth. In this validation, a near-field antenna probe is designed to be placed on the cheek, with known electrical tissue parameters. The temperature of cold water inside the mouth is measured with a thermocouple, and compared to the black-body noise power received by the radiometer.

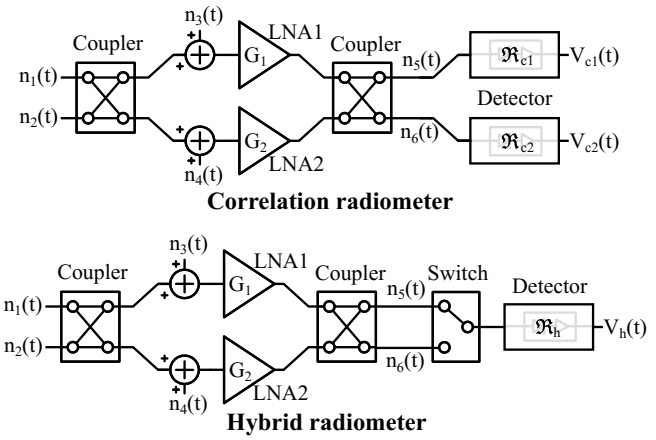

Fig. 2. Block diagrams of correlation and hybrid radiometers, showing noise sources $n_i(t)$. LNA1 refers to the first stage of balanced amplification.

II. Hybrid Radiometer Theory

The radiometer operation can be briefly described as follows, referring to the ports in Fig. 2. The random processes $n_k(t),\ k = 1, \ldots, 6$ are Gaussian-distributed with zero mean, and band-limited to the observation (measurement) bandwidth Δf. The mean power received from the target is $\langle |n_1(t)|^2 \rangle = kT\Delta f$, where k is the Boltzmann constant, and T is the target temperature in K. The reference load is at temperature T_R, so that it delivers a power $\langle |n_2(t)|^2 \rangle = kT_R\Delta f$. The amplifiers (LNA1) add uncorrelated zero-mean Gaussian noise with power $\langle |n_{3,4}(t)|^2 \rangle = kT_{3,4}\Delta f$. These noise sources are added before amplification and thus determine most of the system noise budget.

To show the robustness of the hybrid radiometer against gain fluctuations, suppose the first LNA balanced stage (LNA1) has asymmetric gains $G_1 = G_o + \Delta G_c$ and $G_2 = G_1 + G_d$, where G_o is the mean value, and ΔG_c and ΔG_d common and differential gain fluctuations, respectively. The average noise powers at the output of the second coupler are $\langle |n_{5,6}(t)|^2 \rangle / (k\Delta f) = \frac{1}{4}T_{2,1}(\sqrt{G_1}+\sqrt{G_2})^2 + \frac{1}{2}G_1T_3 + \frac{1}{2}G_2T_4$. In the hybrid radiometer, the noise powers are detected after the switch with a single detector, with a voltage responsivity $\Re_h = \Re_o + \Delta\Re_c$ that fluctuates. For a correlation radiometer, these powers go through separate detectors having common and differential responsivity fluctuations, $\Re_{c1} = \Re_o + \Delta\Re_c$ and $\Re_{c2} = \Re_{c1} + \Delta\Re_d$. The temperature of the target can be estimated from the measured post-detection voltage difference $\Delta V = V_2 - V_1$ as $T^{\text{est}} = \Delta V/(kG_o\Re_o\Delta f) + T_R$. Considering only the effects of gain fluctuations and ignoring higher-order terms, the temperature estimated by the correlation radiometer is $T^{\text{est}} = T + \Delta T$. The uncertainty ΔT can be shown to have the form:

$$\Delta T = \left[\left(\frac{\Delta G_c}{G_o} + \frac{\Delta G_d}{2G_o}\right)\left(1 + \frac{\Delta\Re_c}{\Re_o}\right) + \frac{\Delta\Re_c}{\Re_o}\right](T - T_R) + \frac{\Delta\Re_d}{\Re_o}\left(1 + \frac{\Delta G_c}{G_o} + \frac{\Delta G_d}{2G_o}\right)T + \frac{\Delta\Re_d}{2\Re_o}\left[T_3\left(1 + \frac{\Delta G_c}{G_o}\right) + T_4\left(1 + \frac{\Delta G_d}{G_o}\right)\right]. \quad (1)$$

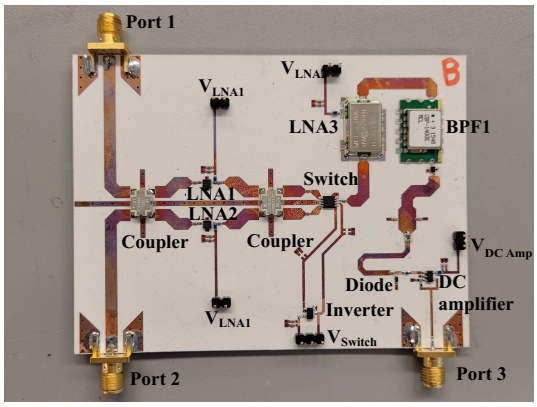

Fig. 3. Photograph of the hybrid radiometer prototype. Off-the-shelf components are used on a 10 cm× 7.6 cm PCB.

Table 1. Components in the designed radiometer.

Component	Manufacturer	Description
Hybrid coupler	Anaren	IL=0.3 dB
LNA1, LNA2	Qorvo	G=16.4 dB, NF= 0.4 dB
Switch	MACOM	IL=0.65 dB
LNA3	Mini-Circuits	G=35 dB, NF= 0.6 dB
BPF1	Mini-Circuits	IL=1.4 dB
BPF2	Tai-saw Tech.	IL=2 dB
Diode(detector)	Skyworks	-
DC amplifier	Diodes Inc.	G=100

Therefore, the gain and responsivity fluctuations originating from flicker noise increase the uncertainty of the estimation [13]. More importantly, that uncertainty does not vanish for a perfectly balanced correlation radiometer ($T = T_R$). One advantage of a hybrid architecture is that $\Delta\Re_d = 0$ because a single detector observes both outputs of the second hybrid coupler by switching faster than the responsivity fluctuations. Besides reducing the overall uncertainty, the hybrid radiometer can be balanced, becoming immune to flicker noise.

III. Radiometer Design and Implementation

Since the noise power received from the body is low compared to other ambient signals at radio frequencies, the radiometer is designed in the 1.4 GHz quiet band allocated to radioastronomy, with a bandwidth of $\Delta f = 27$ MHz. Assuming a temperature of 37°C, the expected total power is $kT\Delta f = -99$ dBm (116 fW). The detector has a sensitivity of -55.5 dBm, and taking into account loss in the filters, switch and couplers, the required total gain is about 43.5 dB. The hybrid radiometer is assembled with OTS components (Table 1). The 10 cm×6.7 cm fabricated circuit on a Rogers 3010 1.27 mm thick substrate is shown in Fig. 3.

The simulated 3-port S-parameters from the RF input ports 1 and 2 to the input of the detector are shown in Fig. 4. The simulated gain before the RF detector is 45.5 dB. The measured input reflection coefficients are also shown and $|S_{11}| < -10$ dB from 0.95-1.7 GHz. The detector is fabricated and characterized separately, with voltage responsivity shown in Fig. 5 and an average responsivity of 4.1 kV/W. The detector

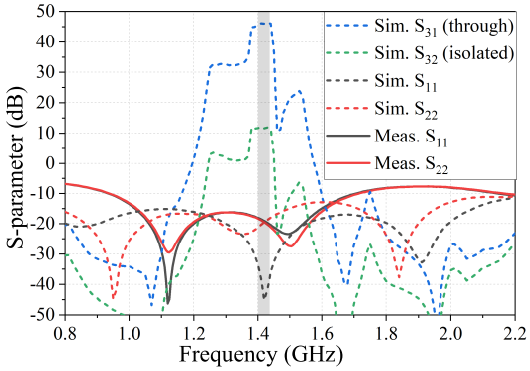

Fig. 4. Simulated (dashed) and measured (solid) S-parameters of the radiometer prototype using components from Table 1. The shaded area indicates the design frequency band.

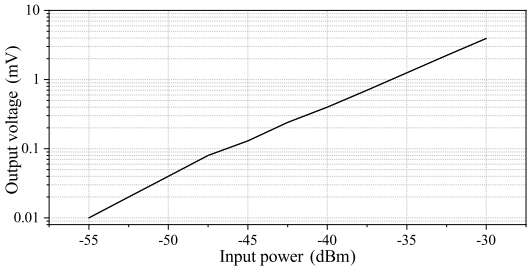

Fig. 5. Measured voltage responsivity of the detector at 1.415 GHz.

diode impedance is $Z_D = 27 - j812\,\Omega$ and is matched using a high-impedance line and shunt capacitors.

IV. Radiometer Calibration and Temperature Estimation

To calibrate the hybrid radiometer, two matched loads at different temperatures T_1 and T_2 are connected to the input ports. Due to the imbalances from the hybrid couplers, amplifiers and switch, the output voltage for the two switch states is a linear combination of inputs at ports 1 and 2:

$$V_1 = \alpha_{11}T_1 + \alpha_{12}T_2 + \alpha_{13} \tag{2a}$$

$$V_2 = \alpha_{21}T_1 + \alpha_{22}T_2 + \alpha_{23}. \tag{2b}$$

Defining $\alpha_i = \alpha_{i1} - \alpha_{i2}$,

$$\Delta V = V_1 - V_2 = \alpha_1 T_1 + \alpha_2 T_2 + \alpha_3. \tag{3}$$

The constant α_i is determined by the different known pairs of T_1 and T_2. In the experiment, 13 temperature pairs are used. α_i values are calculated using linear fitting. T_1 and T_2 are created using two temperature controllable $50\,\Omega$ loads. A chip resistor is placed on a separate board connected with a $50\,\Omega$ transmission line. The circuit is attached to a Peltier thermoelectric cell, controlled by a ThorLabs MTD415T thermistor temperature controller, using thermally conductive tape, with the other side of the Peltier element connected to a heat sink. The structure is thermally isolated using polystyrene foam.

Two different estimation methods for determining temperature T_1 are next compared. Method 1 uses the

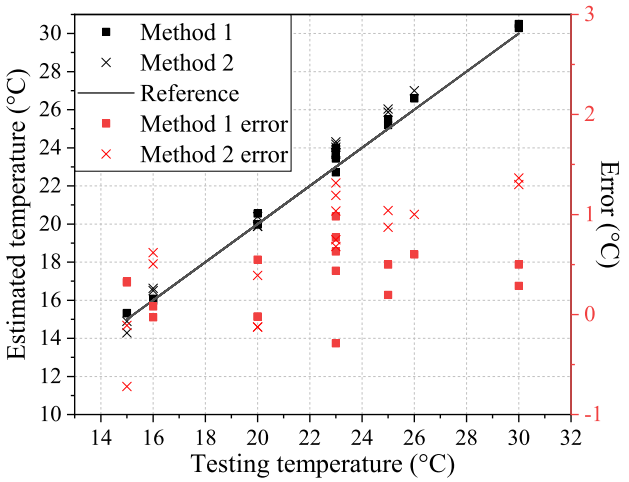

Fig. 6. Measured temperature estimated from two calibration methods, measured on two different days, with and integration time of 5 seconds.

measurement of ΔV at the output of the post-detector amplifier to directly estimate the temperature as:

$$T_1^{\text{est}} = \frac{\Delta V}{\alpha_1} + \frac{\alpha_2}{\alpha_1}T_2 + \frac{\alpha_3}{\alpha_1}. \tag{4}$$

Method 2 dynamically adjusts the reference temperature T_2 so that $\Delta V \approx 0$. This reduces (4) to:

$$T_1^{\text{est}} = \frac{\alpha_2}{\alpha_1}T_2 + \frac{\alpha_3}{\alpha_1} \tag{5}$$

Method 2 reduces the error caused by the gain fluctuation of the components. Quantities α_i vary proportionally to gain fluctuations, so their ratio remains constant [11].

Radiometric temperature measurements are performed to compare the two methods. The temperature controlled load at Port 1 is set to 15°-33°C. Fig 6 shows the estimated temperature and the error. ΔV is an average value integrated over 5 seconds to reduce radiometric uncertainty. The average errors using Method 1 and Method 2 are 0.386 °C and 0.773 °C. In Method 2, the control algorithm for T_2 causes overshoot and residual error in ΔV. Improvement in the algorithm is needed to make $\Delta V \approx 0$ for Method 2 to have lower error.

V. Measurements on the Human Body

Human body measurements are done using temperature-varying tap water inside the cheek. The probe uses a corner-fed rectangular patch topology on a 1.27 mm thick Rogers RO3010 substrate. The near-field probe designed for tissue layers of the cheek [14] is placed on the skin, and the resulting impedance match is shown in Fig.7. We estimate the temperature radiated from each tissue layer from reciprocity, expressing the total noise power as the weighted sum of the powers of the individual layers [7]. The weighting factors are found from the Joule losses, calculated from the electric field and conductivity of the cheek layers, shown in Fig 8.

The two input ports are connected to a reference load and the near-field antenna. The temperature of the reference

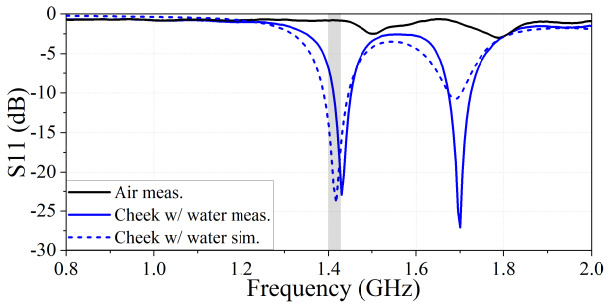

Fig. 7. Measured reflection coefficient magnitude of the near-field antenna when placed on the cheek, comparing the match in air, on the cheek and simulations on the cheek. The shaded area is the design frequency band.

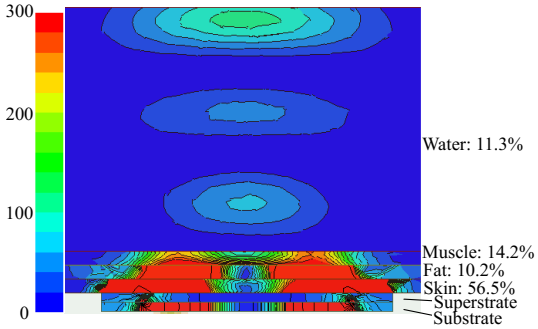

Fig. 8. Full-wave simulations of volume Joule loss density (W/m^3) of the near-field antenna on a cheek tissue stack. The weights (percentage of total power) of cheek tissue layers are also stated.

load is stabilized with a Thorlabs temperature controller. The antenna is attached to the cheek using adhesives and a circulator is used to avoid power fluctuations due to probe mismatch. The measured voltage at the output of the dc amplifier is shown in Fig. 9. ΔV increases linearly with temperature of the water inside the cheek with a responsivity of 0.061 mV/°C. The responsivity with a temperature controllable load is 0.196 mV/°C, so the weighting factor of the water from the measured data is found to be 31 % instead of the 11% obtained from full-wave simulations. We attribute this difference mainly to the variability of electric conductivity in tap water.

VI. Conclusions

A hybrid correlation/Dicke radiometer for measuring internal tissue temperature is demonstrated, and shown to reduce sensitivity to load impedance variations as well as sensitivity to gain fluctuations. The radiometer is designed with OTS components with a total cost of $78 in small quantities. Two types of calibration methods are compared using loads at known controllable temperatures. Human testing uses a near-field antenna probe designed for tissue layers of the cheek. When water of variable temperature is in the mouth, an independent thermocouple verifies the radiometric temperature of the water measured by the probe placed on the skin.

Acknowledgment

This work is supported by the National Science Foundation under award IIP 2044668.

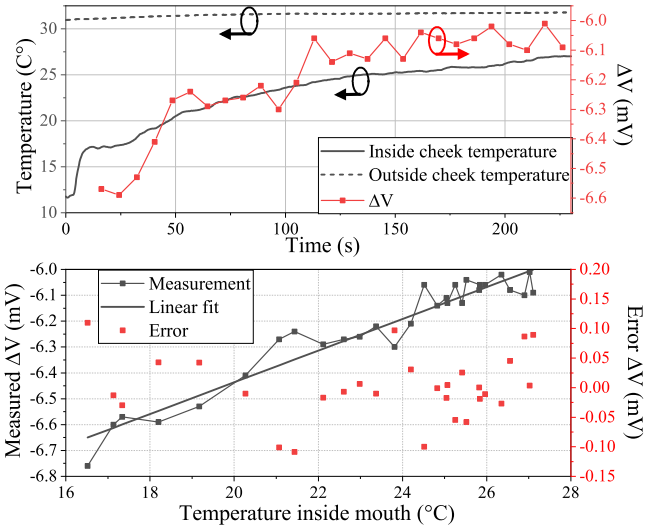

Fig. 9. Top: Measured voltage at output of the radiometer as cold water in the mouth warms up. The temperature is measured with a thermocouple in the mouth. Bottom: Measured ΔV versus time for the same data set, with a linear fit and error of ΔV compared to the measured temperature.

References

[1] F. Biancari *et al.*, "Commentary: Cooling the brain for elective aortic hemiarch repair," *The Journal of thoracic and cardiovascular surgery*, 2021.

[2] G. Baronzio *et al.*, "A brief overview of hyperthermia in cancer treatment," *J Integr Oncol*, vol. 3, no. 115, p. 2, 2014.

[3] L. C. Lack *et al.*, "The relationship between insomnia and body temperatures," *Sleep medicine reviews*, vol. 12, no. 4, pp. 307–317, 2008.

[4] G. Galiana *et al.*, "Accurate temperature imaging based on intermolecular coherences in magnetic resonance," *Science*, vol. 322, no. 5900, pp. 421–424, 2008.

[5] L. Teunissen *et al.*, "Non-invasive continuous core temperature measurement by zero heat flux," *Physiological measurement*, vol. 32, no. 5, p. 559, 2011.

[6] S. Mizushina *et al.*, "Non-invasive temperature profiling using multi-frequency microwave radiometry in the presence of water-filled bolus," *IEICE Trans. on Electronics*, vol. 74, no. 5, pp. 1293–1302, 1991.

[7] P. Momenroodaki *et al.*, "Noninvasive internal body temperature tracking with near-field microwave radiometry," *IEEE Transactions on Microwave Theory and Techniques*, vol. 66, no. 5, pp. 2535–2545, 2017.

[8] V. Levshinskii *et al.*, "Application of data mining and machine learning in microwave radiometry (mwr)," in *Int. Joint Conf. on Biomedical Engineering Systems and Technologies*. Springer, 2019, pp. 265–288.

[9] O. Shevelev *et al.*, "Using medical microwave radiometry for brain temperature measurements," *Drug discovery today*, 2021.

[10] F. T. Ulaby *et al.*, *Microwave radar and radiometric remote sensing*. University of Michigan Press Ann Arbor, MI, USA, 2014, vol. 4, no. 5.

[11] S. G. Vesnin *et al.*, "Portable microwave radiometer for wearable devices," *Sensors and Actuators A: Physical*, vol. 318, p. 112506, 2021.

[12] E. Villa *et al.*, "A 3.5-ghz pseudo-correlation type radiometer for biomedical applications," *AEU - International Journal of Electronics and Communications*, vol. 130, p. 153558, 2021. [Online]. Available: https://www.sciencedirect.com/science/article/pii/S143484112032762X

[13] R. Streeter *et al.*, "Correlation radiometry for subcutaneous temperature measurements," *IEEE Journal of Electromagnetics, RF and Microwaves in Medicine and Biology*, 2021.

[14] C. Gabriel, "Compilation of the dielectric properties of body tissues at rf and microwave frequencies." King's Coll London (United Kingdom) Dept of Physics, Tech. Rep., 1996.